Turk J Chem
33 (2009) , 33 – 45.

doi:10.3906/kim-0808-8

CTAB-Assisted Hydrothermal Synthesis and Magnetic Characterization of $Ni_xCo_{1-x}Fe_2O_4$ Nanoparticles (x = 0.0, 0.6, 1.0)

Abdulhadi BAYKAL[1]*, Nermin KASAPOĞLU[1], Zehra DURMUŞ[1], Hüseyin KAVAS[2], Muhammet S. TOPRAK[3], Yüksel KÖSEOĞLU[2]

[1] *Department of Chemistry, Fatih University, B. Çekmece, 34500 İstanbul-TURKEY*

[2] *Department of Physics, Fatih University, B. Çekmece, 34500 İstanbul-TURKEY*

[3] *Functional Materials Division, Royal Institute of Technology, SE16440 Stockholm- SWEDEN*

Received 20.08.2008

Nickel ferrite, $Ni_xCo_{1-x}Fe_2O_4$, NPs (where x = 0.0, 0.6 and 1.0) were successfully synthesized by a rapid and reproducible CTAB-assisted hydrothermal route. The influence of different hydrolyzing agents on the particle size and magnetic behavior of $Ni_xCo_{1-x}Fe_2O_4$ NPs was investigated. Particles showed very high phase purity and crystallinity in powder XRD analysis. Compositions of Co, Fe, and Ni in fabricated powders were also determined by AAS and results are in very good agreement with the targeted compositions. Samples hydrolyzed using NH_3 showed no significant changes in the particle size and morphology. NH_3 hydrolyzed samples were much smaller than their NaOH hydrolyzed counterparts, which was attributed to the strength and concentration of the hydrolyzing agents, NH_3 being about 6 times more concentrated than NaOH. This in turn influenced the nucleation rate thus the size of each nucleus formed. Strong temperature and Ni concentration dependence of magnetic parameters was observed. These samples are considered as promising materials for high density magnetic recording media.

Key Words: Magnetic materials, Spinels, XRD, Coercivity, Hydrothermal synthesis.

Introduction

Development of spinel ferrite nanoparticles has been intensively pursued because of their technological and fundamental scientific importance due to their magnetic and electronic properties.[1–3]

*Corresponding author

Cobalt ferrite ($CoFe_2O_4$) is a well-known hard magnetic material with high coercivity and moderate magnetization. These properties, along with its great physical and chemical stability, make $CoFe_2O_4$ nanoparticles suitable for magnetic recording applications such as audio and videotape and high-density digital recording disks.[4,5]

Nickel ferrite ($NiFe_2O_4$) has a wide range of applications in many fields including biomedical applications, magnetic refrigeration, magnetic liquids, microwave absorber, repulsive suspension for levitated railway systems and gas sensing capabilities towards low concentrations of chlorine gas, and for catalysts for the benzoylation of toluene with benzyl chloride.[6,7] $NiFe_2O_4$ exhibits unusual physical and chemical properties when its size is reduced to nano-regime. Owing to the extremely small dimensions of nano-structured materials, a major portion of the atoms lies at the grain boundaries, which in turn is responsible for superior magnetic, dielectric, and mechanical properties in these materials compared to their conventional coarse grained counterparts.[8–13]

The magnetic properties of spinel ferrites can be varied systematically by changing the identity of the divalent M^{2+} cations (M = Co, Mn, Ni, Zn, etc.) without changing the spinel crystal structure.[14] It is well known that the chemical, structural, and magnetic properties of ferrite nanoparticles are strongly influenced by their composition and microstructure, which are sensitive to the preparation methodologies.[15] Ferrite nanoparticles have been conventionally prepared by mechanical-milling,[16] hydrothermal method,[17–20] coprecipitation reaction,[21] micro-wave route,[22,24] reverse and normal micelles,[25] reflux method,[26] oxidation-reduction,[27] sol–gel method,[28] microemulsion method,[31–32] surfactant-assisted route,[30,31] and thermal decomposition.[33]

In this work, CTAB-assisted hydrothermal method was used to synthesize $Ni_xCo_{1-x}Fe_2O_4$ nanoparticles and the effect of different hydrolyzing agents was investigated. The effects of CTAB as a transferring agent, and concentrated ammonia and sodium hydroxide as hydrolyzing agents on particle size and morphology were investigated. The synthesized nanocrystalline samples were characterized by X-ray diffraction (XRD), Fourier transform infrared (FTIR) spectroscopy, and transmission electron microscopy (TEM). The magnetic properties of nanoparticles were investigated using a vibrating sample magnetometer (VSM).

Experimental

Measurements

X-ray powder diffraction (XRD) analysis was performed using a Huber JSO-DEBYEFLEX 1001 Diffractometer with Cu K_α radiation.

Fourier transform infrared (FTIR) transmission spectra were taken on a Mattson Satellite Infrared Spectrometer in the range of 4000 to 400 cm^{-1}.

Temperature dependent magnetic measurements were carried out with a Quantum Design Vibrating Sample Magnetometer (VSM) Model 6000.

Transmission Electron Microscopy (TEM) analysis was performed using a Philips-FEI Tecnai G2 T20 at 200 kV accelerating voltage in order to investigate the morphology and crystallinity of the synthesized nanoparticles.

Atomic absorption spectroscopy (AAS, Varian GTA 120 model with GTA 120 unit graphite furnace) was performed in order to assess the metal ion concentration for each composition. Samples were dissolved in HCl and diluted in volumetric flasks prior to AAS analysis.

Synthesis

Nanoparticles of $Ni_xCo_{1-x}Fe_2O_4$ (x = 0.0, 0.6, 1.0) were prepared through a surfactant-assisted hydrothermal process. One gram of cationic surfactant cetyltrimethylammonium bromide (CTAB) was dissolved in 35 ml deionized water to form a clear solution. One gram of ferric chloride hexahydrate ($FeCl_3 6H_2O$) was added into this solution. After 10 min, stoichiometric amounts of $CoCl_2$ and $NiCl_2$ given in Table 1 were introduced into the vigorously stirred solution and deionized water was added to make the total solution volume of 40 ml. pH of the solution was adjusted to 11.0 by the addition of 2M NaOH and conc. NH_3 solution, respectively. The solution mixture was pretreated under an ultrasonic water bath for 30–40 min, thereafter was transferred to a teflon-lined 50 ml autoclave. Hydrothermal synthesis was carried out at 130 °C for 15 h in an oven. Afterwards, the autoclave was allowed to cool to room temperature. The dark precipitate was collected and washed with distilled water. The final powder was then annealed at 500 °C for 5 h.

Table 1. Stoichiometric amounts of metal chlorides (in g) used for the CTAB assisted hydrothermal synthesis of $Ni_xCo_{1-x}Fe_2O_4$.

x (Ni content)	$CoCl_2.6H_2O$	$NiCl_2$	$FeCl_3{\cdot}6H_2O$	CTAB
0.0	0.44	-	1	1
0.6	0.18	0.14	1	1
1.0	-	0.23	1	1

Results and discussion

XRD Measurements

Final product was analyzed by XRD in order to investigate the crystalline phases that are present. X-ray diffraction patterns of $Ni_xCo_{1-x}Fe_2O_4$ (with x = 0.0, 0.6, 1.0) are shown in Figure 1.

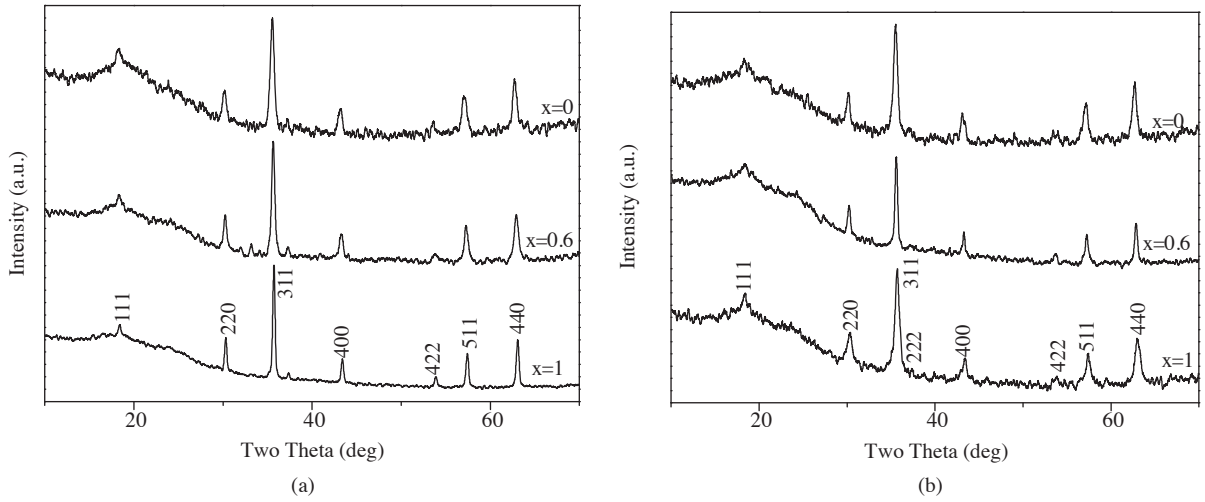

Figure 1. XRD patterns of $Ni_xCo_{1-x}Fe_2O_4$ NPs (x = 0, 0.6, 1) hydrolyzed with: (a) NaOH and (b) NH_3.

The patterns show the reflection planes (111), (220), (311), (222), (400), (422), (511), and (440) that are indications of the presence of the spinel cubic structure.[34] These diffraction lines provide a clear evidence of the formation of a solid solution between $NiFe_2O_4$ and $CoFe_2O_4$. Mixed spinel ferrite was observed for x = 0.6, whereas for x = 0.0 pure $CoFe_2O_4$ (JCPDS file No:22-1086), and for x = 1.0 pure $NiFe_2O_4$ (JCPDS file No:10-325) were formed. Compositions of Co, Fe, and Ni in fabricated powders were also determined by the AAS and results are in a very good agreement with the targeted compositions.

The average particle size of the ferrite particles was determined from the full-width at half maximum (FWHM) of the most intense peak (3 1 1) using the well-known Debye - Scherrer equation:

$$D = 0.9\lambda / B\cos\theta_B$$

where λ is the X-ray wavelength, θ_B is the angle of Bragg diffraction, and B is the full width at half maximum.[29] Results of crystallite size estimated using Debye - Scherrer equation are given in Table 2. Particle size of the samples hydrolyzed using NH_3 decreased by increasing the concentration, x, of Ni in the structure; whereas an increasing size trend was observed with increasing x for samples hydrolyzed using NaOH. Crystallite size was observed to be bigger for samples hydrolyzed using NaOH for a given x.

Table 2. Particle size (nm) of $Ni_xCo_{1-x}Fe_2O_4$ NPs (x = 0.0, 0.6, 1.0) synthesized using different hydrolyzing agents.

Specimen	Particle size (nm) of the specimens	
	2.0 M NaOH	conc. NH_3
$CoFe_2O_4$	35	41
$Ni_{0.6}Co_{0.4}Fe_2O_4$	38	34
$NiFe_2O_4$	60	27

The lattice parameters (Figure 2) were computed using the d-spacings value and the respective (*hkl*) parameters (TREOR Program). The values of lattice parameter found for $NiFe_2O_4$ (a_o = 8.343 (0.001) Å) and for $CoFe_2O_4$ (a_o = 8.381 (0.003) Å) agree with those reported in JCPDS card number 10-325 and 22-1086, respectively. As shown in Figure 2, the lattice parameters decreased linearly with an increase of Ni content (x) suggesting the formation of a compositionally homogeneous solid solution. The unit cell parameter 'a' decreases linearly with the nickel concentration due to smaller ionic radius of nickel. Since the ionic radius of Ni^{2+} is smaller than that of Co^{2+}, the replacement of Co by Ni ions leads to a decrease of the lattice parameter.[33–35] The values of the lattice parameter, "a", exhibit a linear dependence, thus obeying Vegard's law [36] as shown in Figure 2.

X-ray density, Dx, was calculated[37] using the following formula: Dx = 8M / Na^3 where M, N, and a are the molecular weight, Avogadro's number, and the lattice parameter, respectively. Density increases linearly with nickel concentration (Figure 2) since nickel atom is heavier than cobalt atom.

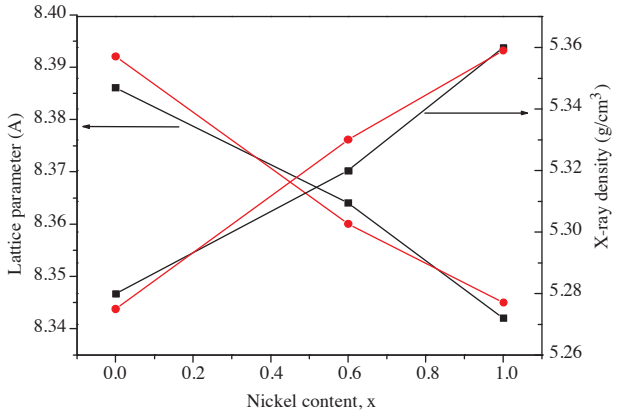

Figure 2. Variation of lattice parameter, and density of $Ni_xCo_{1-x}Fe_2O_4$ NPs (x = 0.0, 0.6, 1.0) (hydrolyzed with NaOH (red line) and NH_3 (black line)) vs. nickel concentration.

FTIR measurements

In the range of 1000-100 cm^{-1}, the IR bands of solids are usually attributed to the vibration of ions in the crystal lattice.[38] Two main metal-oxygen bands are seen in the IR spectra of all ferrites. The highest one, ν_1, observed at 603 cm^{-1} (Figure 3), corresponds to intrinsic stretching vibrations of the metal at the tetrahedral site, $M_{tetra} \leftrightarrow O$, whereas ν_2, the lowest band, usually observed in the range of 450-385 cm^{-1}, is assigned to octahedral-metal stretching, $M_{octa} \leftrightarrow O$.[30,39] These bands for $Ni_xCo_{1-x}Fe_2O_4$ samples were observed around 603 cm^{-1} and 450 cm^{-1}, respectively. No peaks were observed due to CTAB since all prepared NPs were treated at 500 °C to increase the crystallinity of the particles.

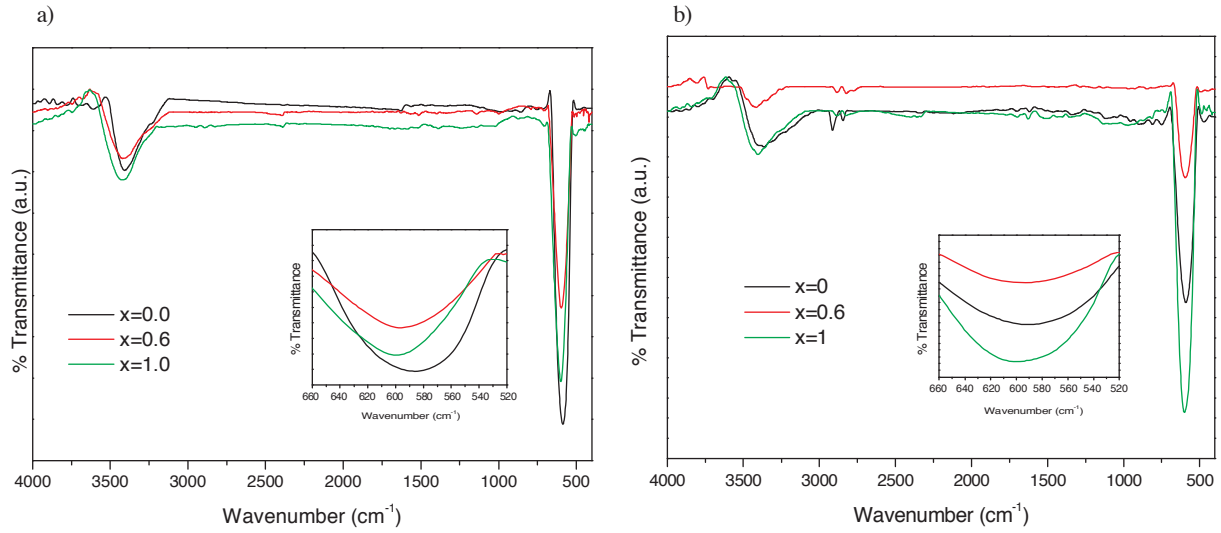

Figure 3. FTIR spectra of $Ni_xCo_{1-x}Fe_2O_4$ NPs (x = 0.0, 0.6, 1.0) hydrolyzed with: (a) NaOH and (b) NH_3.

TEM measurements

TEM analysis was performed to investigate the morphology of the obtained NPs. Samples hydrolyzed using NaOH (Figure 4a) show an increase in the particle size as well as change in their morphology from near spherical to more edgy crystallites (polygons) by increasing Ni content.

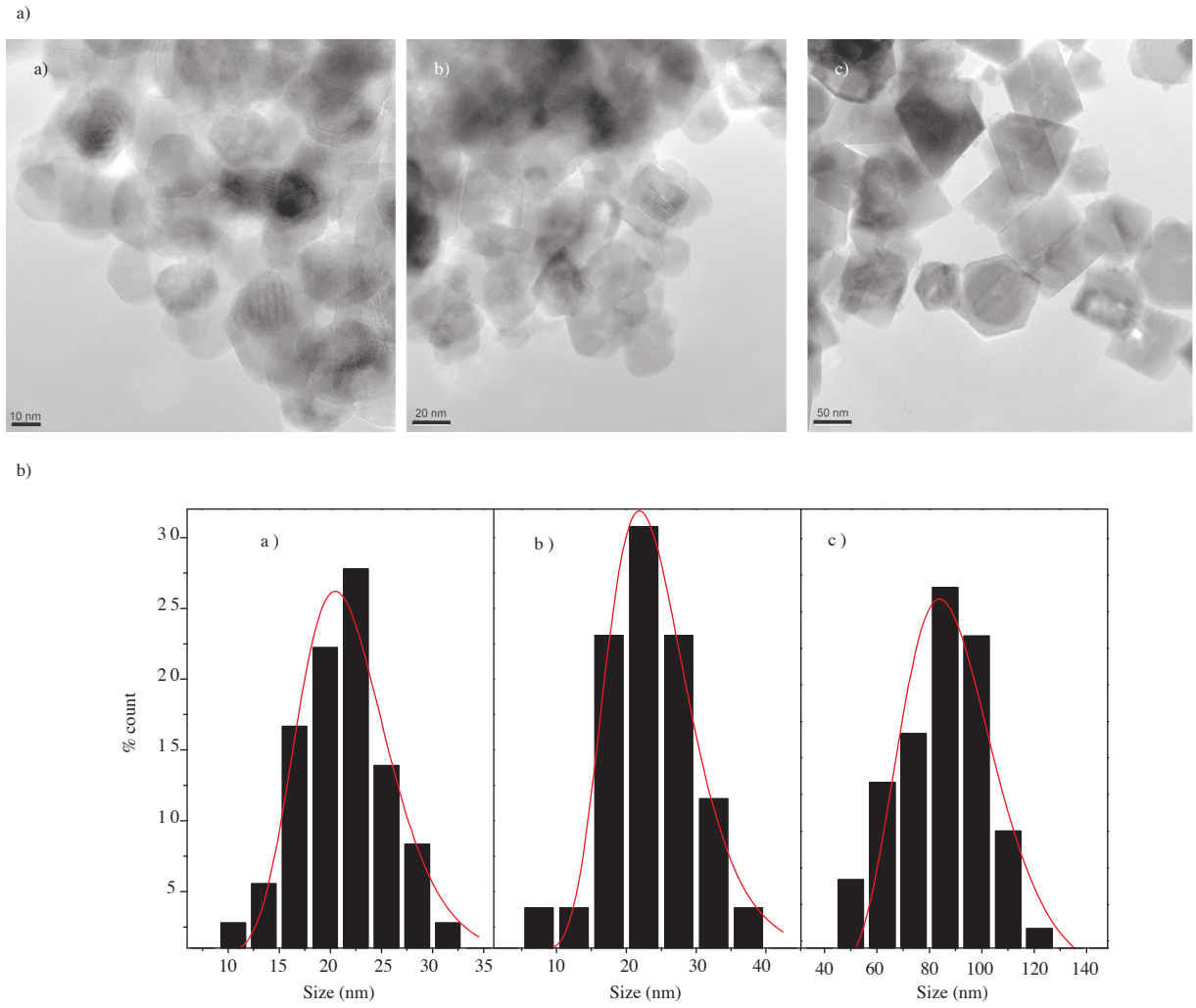

Figure 4. **a)** TEM micrographs of samples hydrolyzed by NaOH with the composition $Ni_xCo_{1-x}Fe_2O_4$ where x is **(a)** 0.0, **(b)** 0.6, and **(c)** 1.0. b) Size distribution histograms and log normal fits for $Ni_xCo_{1-x}Fe_2O_4$ NPs (x = 0, 0.6, 1) hydrolyzed with NaOH.

Samples hydrolyzed using NH_3 (Figure 5a.) show no significant changes in the particle size and morphology. NH_3 hydrolyzed samples are much smaller than their NaOH hydrolyzed counterparts, which becomes significant when x is 1.0. This difference is due to the difference in the strength and concentration of hydrolyzing agents, NH_3 being about 6 times more concentrated than NaOH. This in turn influences the nucleation rate thus the size of each nucleus formed.

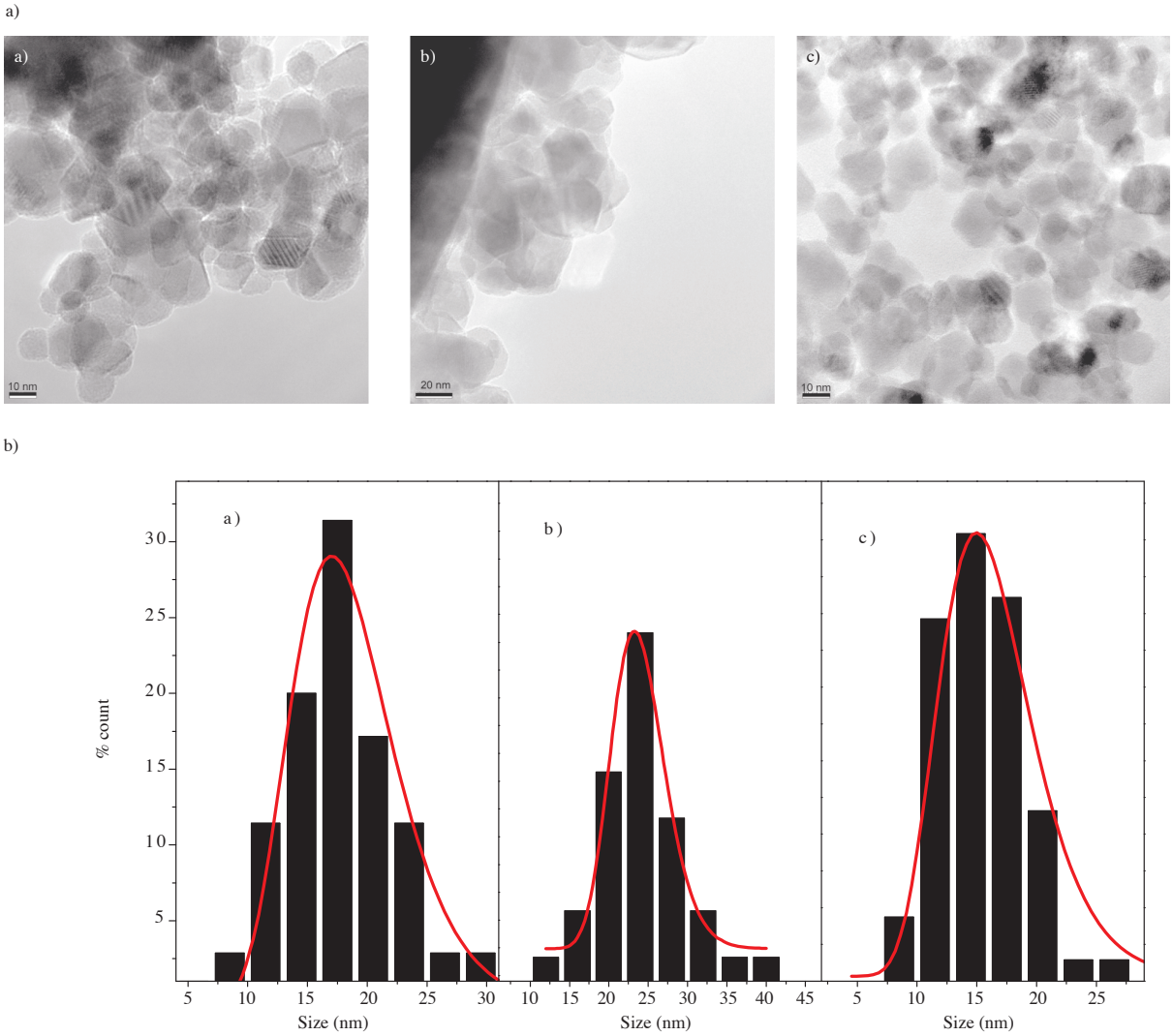

Figure 5. a) TEM micrographs of samples hydrolyzed by NH_3 with the composition $Ni_xCo_{1-x}Fe_2O_4$ where x is (a) 0.0, **(b)** 0.6, and (c) 1.0. b) Size distribution histograms and log normal fits for $Ni_xCo_{1-x}Fe_2O_4$ NPs (x = 0.0, 0.6, 1.0) hydrolyzed with NH_3.

TEM micrographs of as-synthesized Ni-Co ferrite nanoparticles are given in Figures 4a and 5a for NaOH and NH_3 hydrolyzed samples, respectively. Their particle size distribution is presented in Figures 4b and 5b. The size distribution histograms are fitted by using a log-normal function[40] as follows:

$$P(D) = \frac{A}{D\sigma_D\sqrt{2\pi}} \exp\left(-\frac{1}{2\sigma_D^2}\ln(\frac{D}{D_{TEM}})\right) \quad (1)$$

where σ is the standard deviation of the diameter and D_{TEM} is the average diameter obtained from TEM results, which are summarized in Table 2.

TEM size estimate is found by log-normal fitting to the histogram obtained by measuring at least 200 nanoparticles. Crystallite sizes obtained from XRD are smaller than the sizes calculated from TEM. Actually,

the particle size obtained from XRD is the crystallite size but TEM gives the particle size. The reason for this discrepancy is that each particle consists of more than one crystallite. In summary, the crystallite size estimates obtained from different analytical methods are reasonable for the synthesized $NiCo_{1-x}Fe_2O_4$ NPs.

Magnetization measurements

Magnetization measurements of $Ni_xCo_{1-x}Fe_2O_4$ samples hydrolyzed by NH_3 and NaOH were performed using the VSM technique and the M-H curves of the samples at selected temperatures are presented in Figure 6. As can be seen from M-H curves, while the magnetization and the coercivity of the samples increase with the decrease in temperature, they decrease with the increase in Ni content. The decrease in the coercivity and magnetization of the samples with Ni content can be attributed to the anisotropic properties of Co.

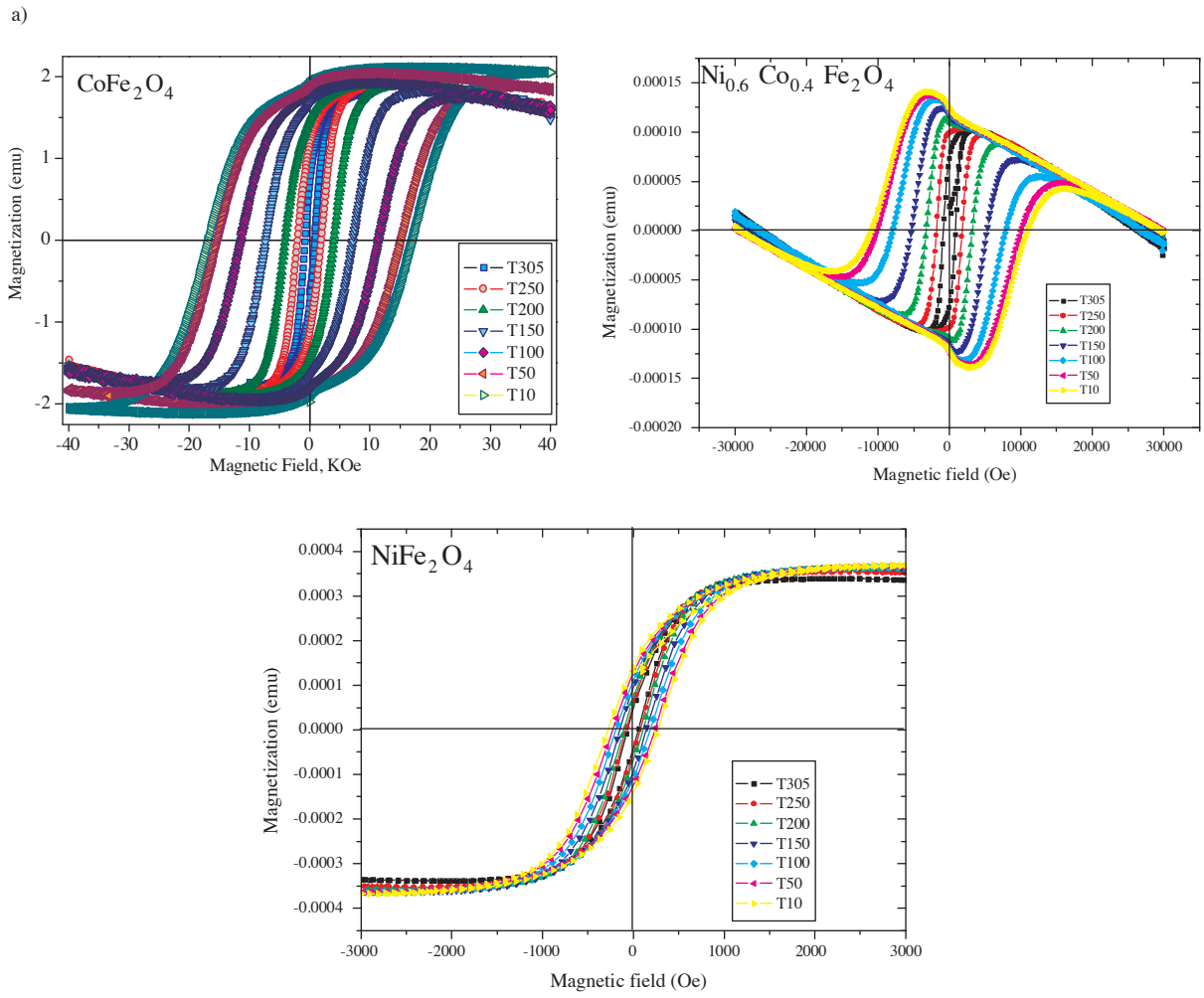

Figure 6. Magnetic hysteresis graphs of $Ni_xCo_{1-x}Fe_2O_4$ NPs (x = 0.0, 0.6, 1.0) hydrolyzed by **a)** NaOH **b)** NH_3 at some selected temperatures.

b)

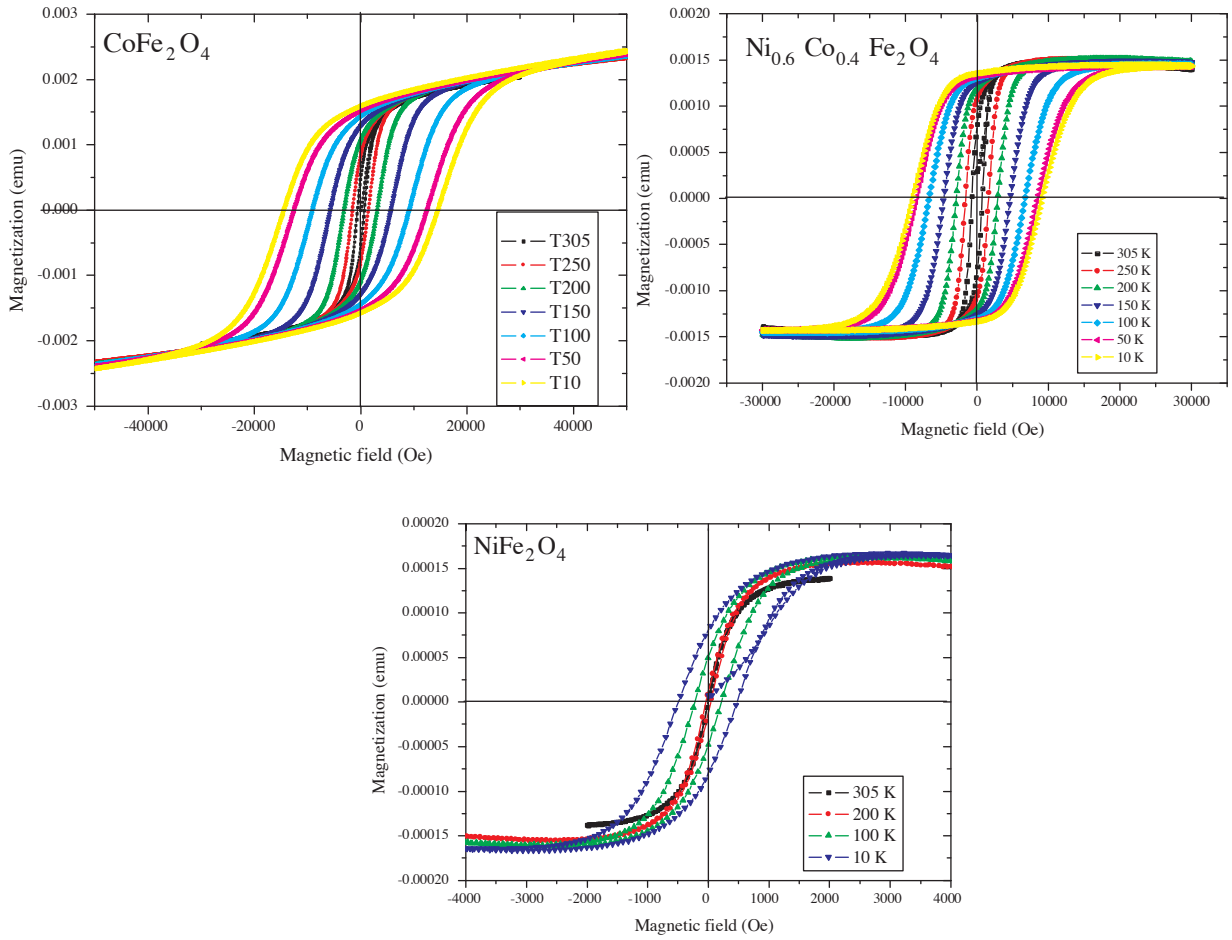

Figure 6. Contunied.

Figure 7 shows the temperature and Ni concentration dependent coercivity of samples hydrolyzed by NH_3 and NaOH, respectively. Coercivity of the samples is strongly temperature dependent. As the temperature decreases, the coercivity of the samples increases and it is more significant in x = 0.0 case. As the Ni concentration increases, the coercivity of the samples decreases for both cases. A decrease in coercivity with an increase in nickel concentration may be attributed to the decrease in the anisotropy field, which in turn decreases the domain wall energy.[41] It is observed that the coercivity of the sample hydrolyzed by NaOH is greater than that of the sample hydrolyzed by NH_3.

It can be observed in Figure 7 that the increase in the coercive field of $CoFe_2O_4$ is much greater, and $CoFe_2O_4$ forms an inverse spinel structure with very high anisotropy energy constants, K_1 and K_2. It is also sensitive to temperature in the lower temperature region. It can be attributed to random freezing of NPs in locally canted states, for which the random anisotropy energy will act as a pinning potential.[24]

In the present case, as the Co^{2+} in $CoFe_2O_4$ grains are substituted by Ni^{2+}, the antiferromagnetic interaction decreases, and the superexchange interaction increases, which leads to a decrease in coercivity and reduced magnetization.[23] As all of Co^{2+} ions are replaced by Ni^{2+} ions, both coercivity and reduced

magnetization reduces too much.

The coercivity of a magnetic material is generally a measure of its magnetocrystalline anisotropy. However, the dramatic increase in low-temperature coercivity cannot be attributed only to magnetocrystalline anisotropy alone. It may originate from exchange anisotropy due to spin disorder at the particles' surface at low temperatures. The effect is expected to be larger for smaller particles due to the increase in the surface-to-volume ratio as observed in the present case.

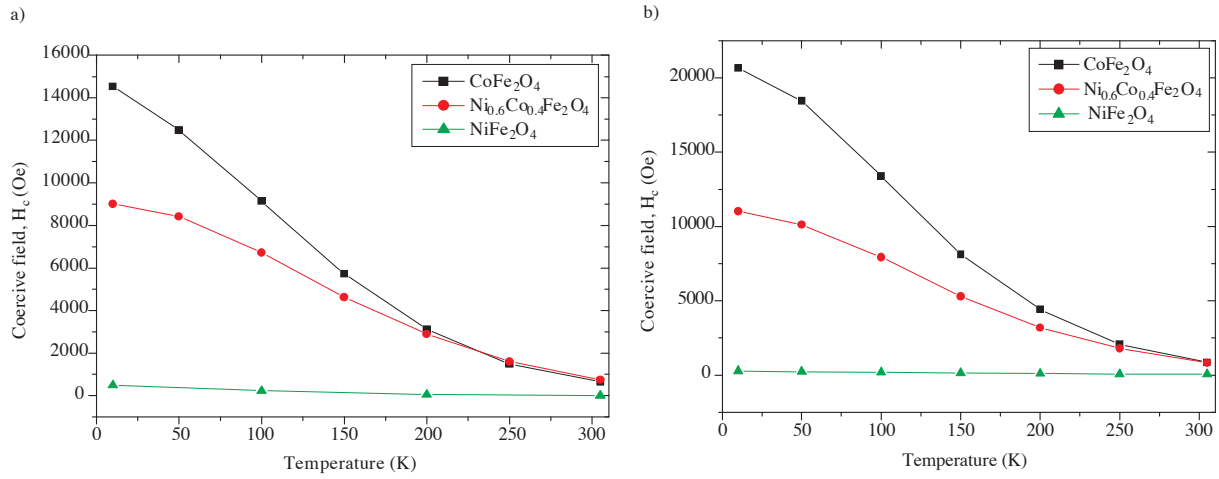

Figure 7. Coercive field vs. Temperature of $Ni_xCo_{1-x}Fe_2O_4$ (x = 0.0, 0.6, 1.0) NPs hydrolyzed with: (a) NaOH and (b) NH_3.

Reduced magnetizations (Mr/Ms) with respect to the temperature of all samples are shown in Figure 8. While the temperature decreases, the reduced magnetization increases for all samples. When the Ni concentration increases, the reduced magnetization decreases. The increase in reduced magnetization indicates the hysteric loop of the sample is evolving toward the square loop. When the reduced magnetization is higher, the sample is a good candidate for magnetic recording. A decrease of reduced magnetization and coercivity with a decrease in cobalt concentration can be understood by the fact that, due to relatively high orbital contribution to magnetic moment, Co^{2+} ions are known to give large induced anisotropy.

Since the reduced magnetization becomes higher (Figure 8), the hysteresis loop evolves towards a square form when the temperature decreases below the blocking temperature in the ferromagnetic material as cobalt ferrites. Such an increase turns out to be more significant than the increase of the Co anisotropy, which could be related to the progressive blocking of the grains having sizes smaller than that of the grains being blocked at 300 K. In fact, the temperature dependence of the domain wall width corresponds to a monotonic decrease with temperature.[42] Squareness of the samples hydrolyzed by NaOH is more significant than that of the samples hydrolyzed by NH_3.

In the cubic system of ferrimagnetic spinels, the magnetic order is mainly due to a super-exchange interaction mechanism occurring between the metal ions in the A and B sublattices. The change in Ms, Hc, and Mr are due to the formation of a dead layer on the surface, existence of random canting of particle surface spins, non-saturation effects due to random distributions of particle size, deviation from the normal cation

distribution, and the presence of adsorbed water. All these factors may reduce the magnetic properties of nanoparticles. The deviation of cation distribution in nanoparticles from bulk also influences the temperature dependence of magnetization.

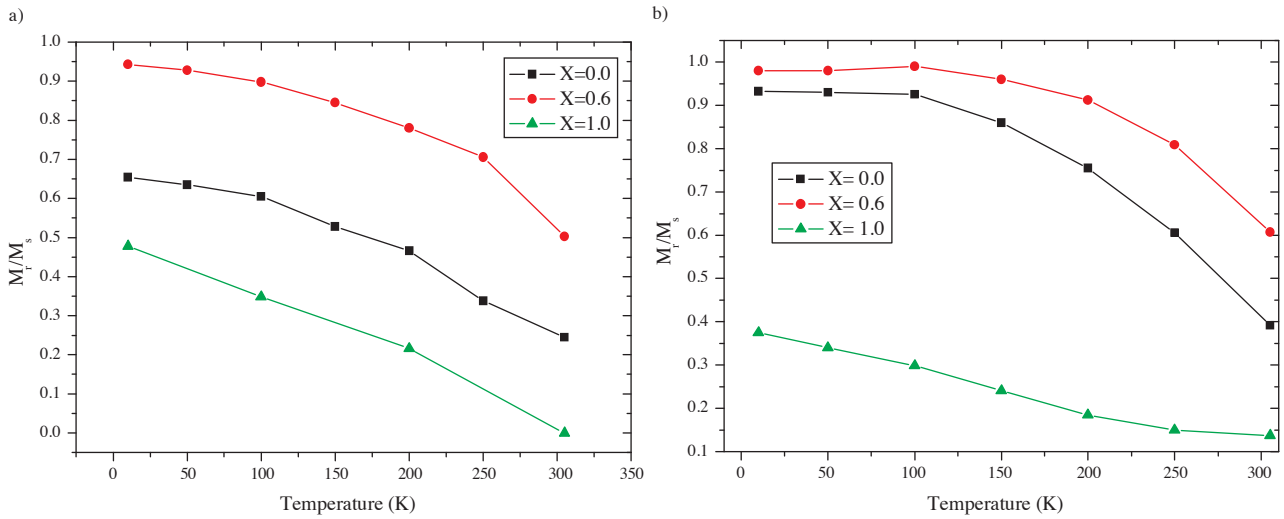

Figure 8. Mr/Ms curves for $Ni_xCo_{1-x}Fe_2O_4$ NPs (x = 0.0, 0.6, 1.0) hydrolyzed with: (a) NaOH and (b) NH_3.

Conclusion

A rapid and reproducible CTAB-assisted hydrothermal route is presented for the synthesis of ferrite magnetic materials with high purity and high yield. Specifically, $Ni_xCo_{1-x}Fe_2O_4$ NPs (where x = 0.0, 0.6, and 1.0) were successfully synthesized by this method. The influence of different hydrolyzing agents on the particle size and magnetic behavior of $Ni_xCo_{1-x}Fe_2O_4$ NPs were investigated. Particles showed very high phase purity and crystallinity in powder XRD analysis and their atomic composition was confirmed by AAS. A strong dependence of magnetic parameters on the temperature and Ni concentration were observed. The changes in Ms, Hc, and Mr are due to the influence of the cationic stoichiometry and their occupancy in the specific sites, dead layer on the surface, existence of random canting of particles surface spins, non-saturation effects due to random distribution of particle size, and the presence of adsorbed water. Coercivity of $CoFe_2O_4$ NPs increased drastically at low T, reaching much higher values than that of bulk. This is mainly attributed to the exchange anisotropy due to spin disorder at the particles' surface caused by the increase in the surface-to-volume ratio. These samples are good candidates for high density magnetic recording media.

Acknowledgements

The authors are thankful the Fatih University Research Project Foundation (Contract no: P50020602) for financial support and Dr. M. S. Toprak acknowledges the fellowship from Knut and Alice Wallenbergs Foundation (No:UAW2004.0224).

References

1. Alivisatos, A.P.; *Science* **1996**, *271*, 933-937.
2. Sugimoto, M. *J. Am. Ceram. Soc.* **1999**, *82*, 269-280.
3. Rondinone, A.J.; Samia, A.C.S.; Zhang, Z.J. *Appl. Phys. Lett.* **2000**, *76*, 3624-3626.
4. Pallai, V.; Shah, D.O. *J. Magn. Magn. Mater.* **1996**, *163*, 243-248.
5. Skomski, R. *J. Phys. Condens. Matter.* **2003**, *15*, R841-934.
6. Ramankutty, C.G.; Sugunan, S. *Appl. Catal. A* **2001**, *218*, 39-51.
7. Reddy, C.V.G.; Manorama, S.V.; Rao,V.J. *Sens. Actuators B:Chemical* **1999**, *55*, 90-95.
8. Zhou, Z.H.; Wang, J,M,; Chan, H.S.O.; Yu T., Shen, Z.X. *J. Appl.Phys.* **2002**, *91*, 6015-6020.
9. Candlish, I.E.; Kear, B.H.; Kim, B.K. *Nanostuct. Mater* **1992**, *1*, 119-124.
10. Skandan, G.; Hahn, H.; Roddy, M.; Cannon, W.R. *J Am. Ceram. Soc.* **1994**, *77*, 1706-1710.
11. Kishimoto, M.; Sakurai, Y.; Ajima, T. *J. Appl. Phys.* **1994**, *76*, 7506-7509.
12. Chen, Q.; Zhang, Z.J. *Appl. Phys. Lett.* **1998,** *73*, 3156-3158.
13. Music, S.; Popovic, S.; Dalipi, S. *J. Mat. Sci.* **1993,** *28*, 1793-1798.
14. Liu, X.M.; Yang, G.; Fu, S.Y. *Mater. Sci. Eng. C* **2007,** *27(4)*, 750-755.
15. Li, F.; Liu, J.J.; Evans, D.G.; Duan, X. *Chem. Mater.* **2004,** *16*, 1597-1602.
16. Goya, G.F.; Rechenberg, H.R. *J. Magn. Magn. Mater.* **1999,** *196*, 191-192
17. Kasapoğlu N., "Synthesis, Characterization and ESR Studies of Magnetic Spinel Compounds, Master Thesis, Fatih Univ., 2008, İstanbul-TURKEY.
18. Kasapoğlu, N.; Birsöz, B.; Baykal, A.; Köseoğlu, Y.; Toprak, M.S. *Cent. Eur.J. Chem.* **2007,** *5(2)*, 570-580.
19. Baykal, A.; Kasapoğlu, N.; Köseoğlu, Y.; Toprak, M.S.; Bayrakdar, H. *J. Alloys Compounds* **2008**, *464*, 514-518.
20. Sertkol, M., "Preparation and Magnetic Characteization of Microwave Absorbing Magnetic Materials", Master Thesis, Fatih Univ., 2008, İstanbul-TURKEY.
21. Sertoğlu, M.; Köseoğlu, Y.; Baykal, A.; Kavas, H.; Başaran, A.C. *J. Magn. Magn. Mater.* **2009**, *321,* 157-162.
22. Ozkaya, T., "Synthesis and Characterization of M_3O_4 (M:Fe,Mn,Co) Magnetic Nanoparticles", Master Thesis, Fatih Univ., 2008, İstanbul-TURKEY.
23. Baykal, A.; Kasapoğlu, N.; Köseoğlu, Y.; Başaran, A.C.; Kavas, H.; Toprak, M.S. *Cent. Eur.J. Chem.* **2008,** *6(1)*, 125-130.
24. Kasapoglu, N.; Baykal, A.; Koseoglu, Y.; Toprak, M.S. *Scripta Mater* **2007,** *57*, 441-444.
25. Lee, Y.; Lee, J.; Bae, C.J.; Park, J.G.; Noh, H.J.; Park, J.H.; Hyeon, T. *Adv. Funct. Mater.* **2005,** *15*, 503-509.
26. Ozkaya, T.; Toprak, M.S.; Baykal, A.; Kavas H.; Köseoğlu Y.; Aktaş, B. *J.Alloys and Compounds* **2008,** doi:10.1016/j.jallcom.2008.04.101.
27. Ozkaya, T.; Baykal, A.; Kavas, H.; Köseoğlu, Y.; Toprak, M.S. *Physica B.* **2008,** *403*, 3760-3764.
28. Liu, X.M.; Fu, S.Y.; Huang, J. *Mater. Sci. Eng. B* **2005,** *121*, 255-260.
29. Chae, K.P.; Lee, J.; Kweon, H.S.; Lee, Y.B. *J. Magn. Magn. Mater.* **2004,** *283*, 103-108.

30. Kasapoğlu, N.; Baykal, A.; Toprak, M.S.; Köseoğlu, Y.; Bayraktar H. *Turk.J. Chemistry* **2007,** *6*, 659-666.
31. Sertkol, M.; Köseoğlu, Y.; Baykal A.; Kavas, H.; Başaran, A.C. *J. Magn. Magn. Mater.* **2009**, *321,* 157-162.
32. Köseoğlu, Y.; Baykal, A.; Toprak, M.S.; Gözüak, F.; Başaran, A. C.; Aktaş, B. *J. Alloys Compounds* **2008,** *462*, 209-213.
33. Özkaya T.; Baykal A.; Toprak M.S. *Cent. Eur. J. Chem.* **2008,** *6(3)*, 465-469.
34. El Sayed, A.M. *Ceram. Int.* **2002,** *28*, 363-367.
35. Sousa, M.H.; Tourinho, F.A. *J. Phys. Chem. B* **2001,** *105*, 1168-1175.
36. Gupta, N.; Verna, A.; Kashyap, S.C.; Dube, D.C. *J. Magn. Magn. Mater.* **2007,** *308*, 137-142.
37. Cullity, B.D. *Elements of X-ray Diffraction*, 3^{rd} Edition, Prentice Hall, New York, 2001.
38. Brabers. V.A.M. *Phys. Status Solidi (a)* **1972,** *12*, 629-636.
39. Hanh, N.; Quy, O.K.; Thuy, N.P.; Tung, L.D.; Spinu. L. *Physica B* **2003,** *327*, 382.
40. T. Kim, and M. Shima, J. Appl. Phys. **2007**, *101*09M516.
41. Kools, F.; Hanket, B. Proc ICF-5 **1989,** *1*, 417.
42. Wohlfarth, E.P. *Ferromagnetic Materials*, Wiley-VCH, Amsterdam, 1980.